

Article

A Process Intensification Approach for CO₂ Absorption Using Amino Acid Solutions and a Guanidine Compound

Abishek Kasturi ^{1,2}, Jorge F. Gabitto ^{3,*} , Radu Custelcean ¹ and Costas Tsouris ^{1,2,*} 

¹ Oak Ridge National Laboratory, Oak Ridge, TN 37831, USA; abishek_kasturi@gatech.edu (A.K.); custelceanr@ornl.gov (R.C.)

² School of Civil and Environmental Engineering, Georgia Institute of Technology, Atlanta, GA 30332, USA

³ Department of Chemical Engineering, Prairie View A&M University, Prairie View, TX 77446, USA

* Correspondence: jfgabitto@pvamu.edu (J.F.G.); tsourisc@ornl.gov (C.T.)

Abstract: Environmentally friendly amino-acid salt solutions are used for the absorption of carbon dioxide from concentrated flue-gas streams via chemical absorption. Process intensification reduces operating and capital costs by combining chemical reactions and separation operations. Here, we present a new process-intensification approach that combines the CO₂ capture and the amino-acid regeneration steps into a single process carried out in a slurry three-phase reactor. The absorbed CO₂ precipitates as a solid carbonated guanidine compound. The cycle is completed by separation of the solid precipitate to strip the CO₂ and regenerate the guanidine compound, while the liquid solution is recycled to the slurry reactor. The process was studied by modifying a model developed by the authors for a gas-liquid bubble column without the presence of the guanidine compound. The guanidine precipitation reaction was accounted for using kinetic parameters calculated by the authors in another study. The proposed model was implemented by modifying an existing computer code used for the simulation of gas-liquid bubble columns. The calculated results showed that the proposed cycle can significantly reduce energy, equipment, and operating costs and can make an important contribution to developing a competitive cost-effective large-scale process for CO₂ capture.

Keywords: CO₂ absorption; amino acids; process intensification; slurry bubble column



Citation: Kasturi, A.; Gabitto, J.F.; Custelcean, R.; Tsouris, C. A Process Intensification Approach for CO₂ Absorption Using Amino Acid Solutions and a Guanidine Compound. *Energies* **2021**, *14*, 5821. <https://doi.org/10.3390/en14185821>

Academic Editor:
Giovanni Lutzenberger

Received: 1 August 2021
Accepted: 7 September 2021
Published: 14 September 2021

Publisher's Note: MDPI stays neutral with regard to jurisdictional claims in published maps and institutional affiliations.



Copyright: © 2021 by the authors. Licensee MDPI, Basel, Switzerland. This article is an open access article distributed under the terms and conditions of the Creative Commons Attribution (CC BY) license (<https://creativecommons.org/licenses/by/4.0/>).

1. Introduction

The effects of climate change can be decreased only by major reductions in anthropogenic CO₂ emissions [1–3]. One of the most important industrial processes for carbon dioxide capture is chemical absorption by amines or blends of different amines as absorption solvents ([4–8], among others). A stripping step that regenerates the solvents and releases the CO₂ completes a separation cycle. The most important shortcomings of the process are the high energy budget required for CO₂ stripping [4] and the toxicity of some of the solvents used [7].

Recently, many authors have studied the use of amino acid salt solutions as absorbents for CO₂ sequestration [9–16], among others. Several authors reported the kinetics of CO₂ absorption by amino acid salt solutions [9–13]. Values of the kinetic parameters have been experimentally determined using the stopped flow technique [14,15]. Other researchers studied different processes using different contactors to increase the mass transfer rate between the gas and liquid phases [16,17].

Amino acid salt solutions present several advantages over traditionally used solvents. For example, aqueous amino acid solutions are less volatile, less corrosive, and more stable to oxidation than most amine solvents [15,18].

There is a need to design economic and efficient industrial processes that allow successful implementation of these novel concepts. Gabitto et al. [19] presented dynamic models for CO₂ absorption in a two-phase batch reactor and in a bubble column reactor. The authors also reported a complete reaction scheme for the different chemical species

participating in the process. Gabitto et al. [19] implemented computationally the developed models and discussed some applications for design, optimization, and control purposes.

Kasturi et al. [17] experimentally and theoretically studied the CO₂ absorption from flue gas streams produced in power-plants using amino acid salt solutions. The authors studied the process using a bubble column contactor. The main process parameters, e.g., bubble size, liquid-phase dispersion coefficient, and gas hold-up were experimentally determined. Kasturi et al. [17] used Gabitto et al.'s model [19] to simulate the two-phase bubble reactor operation. The simulation results agreed well with equivalent experimental data. Brethomé et al. [16] reported a process for direct CO₂ absorption from air using glycine and sarcosine alkaline salt solutions. A complete cycle was proposed by reaction of the produced heavy carbonated solutions with a guanidine compound. This compound crystallizes as a very insoluble carbonate salt and regenerates the amino acid sorbent [16]. This process significantly reduces energy demand because the regeneration step is carried out by light heating of a solid instead of the entire bulk solution. Stripping of the captured CO₂ to regenerate the liquid solvents is an energy intensive process typically used in industrial operations [4]. Some studies confirmed that the use of guanidine compounds can significantly reduce the energy budget of the regeneration process and lead to the design of energy-efficient and cost-effective carbon-sequestration technologies [16,20,21]. These research projects studied the chemistry of several guanidine compounds that crystallize as heavily carbonated precipitates. These carbonated compounds can release the CO₂ and regenerate the original guanidine compound by only light heating (120 °C) in an oven. Williams et al. [21] reported that the minimum energy required for the regeneration of glyoxal-bis(iminoguanidine) (GBIG) is 151.5 kJ/mol CO₂. This value is 24% lower than the regeneration energy of MEA, a typical industrial sorbent. Kasturi et al. [22] experimentally and theoretically studied the glycine regeneration by crystallization of a heavy carbonated guanidine compound (GBIGH₂²⁺(HCO₃⁻)₂(H₂O)₂). The authors developed a simulation model and determined the regeneration mechanism by comparing model predictions and experimental data. Kasturi et al. [22] concluded that the thermodynamic driving force for the glycine regeneration is provided by the GBIGH₂²⁺ bicarbonate crystallization step while the rate-limiting step is the protonation of GBIG to form GBIGH₂²⁺.

Process intensification, a new subject in process engineering, is focused on reducing operating and capital costs by combining reaction and separation operations [23]. The goal of this research project is to present a novel process-intensification approach that combines the CO₂ absorption and the amino-acid regeneration steps into a single process carried out in a slurry three-phase bubble column.

2. Materials and Methods

2.1. Model Organization

A similar approach to the one used by Gabitto et al. [8,19] in their simulation of the absorption/desorption of carbon dioxide in a gas-liquid bubble column will be followed. First, a reaction mechanism will be proposed. Second, a process model for a three-phase (gas-liquid-solid) bubble column will be presented. Finally, the reaction mechanism will be combined with the process model to simulate CO₂ capture in the slurry bubble column.

2.2. Reaction Scheme

In this section we present a summary of the most important reactions to be considered. In the Appendix we present all the reactions involved. A detailed analysis of the mechanism can be found in Gabitto et al. [19]. One important part of the proposed model is the formulation of the chemical reactions involving the amino acid salts, the solvents, and CO₂. Kasturi et al. [22] found that glycine suffers non-negligible decomposition during the heating process; therefore, a more stable amino acid salt, sarcosine, was used in this work. The reaction of sarcosine (CH₃NHCH₂CO₂H) with CO₂ has been studied by several

authors [10,24,25]. A two-step mechanism has been proposed. The first step leads to the formation of a zwitterion intermediate:



Equation (1) is considered the rate controlling step. It is followed by a proton transfer to a base [19]:



All bases present in the liquid phase will participate in reaction (2). For high amino acid concentration, the rate expression simplifies to [26]:

$$r_1 = k_1[\text{CO}_2] [\text{CH}_3\text{NHCH}_2\text{COO}^-] \quad (3)$$

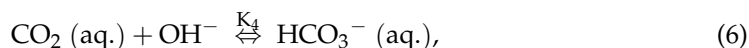
Equation (1) is considered the main reaction in the absorption of CO_2 in high concentration aqueous amino acid solutions. The amino acid salts (anions) also react reversibly with bicarbonate to generate carbamate ions by [25],



Protonated and non-protonated carbamate ions follow the equilibrium given by:

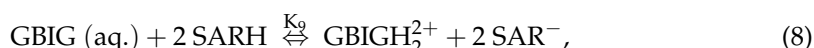


CO_2 can also react with other bases present in the solution, OH^- and H_2O for example, by,

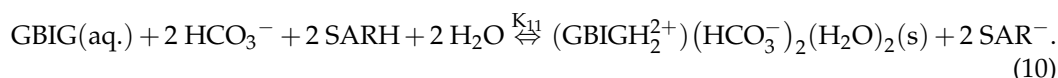


Reaction (6) is the main reaction in alkaline aqueous solutions. Reaction (7) is very slow and makes a negligible contribution to CO_2 absorption in most cases [4,10].

Kasturi et al. [22] found that in the presence of sarcosine, GBIG crystallizes as a heavily carbonated precipitate by the following mechanism:



All bases in the liquid phase compete to protonate GBIG. The weakest base (strongest conjugated acid) will donate the proton. In the case of water, the base is OH^- , and the conjugated acid is H_2O ($\text{pK}_a = 14$). Amino acids, pK_a about 9–10, are far weaker bases than OH^- , thus the amino acid donates the proton to the guanidine compound. The rate-limiting process is the hydrogenation of GBIG, Equation (8), while Equation (9) provides the thermodynamic driving force for the regeneration process. The global reaction is given by:



In the reaction scheme the overall rates of reaction (R_{ai}) were calculated using,

$$R_{ai} = r_{fi} - r_{ri} \quad (11)$$

Here, r_{fi} and r_{ri} are the forward and reverse reaction rates, respectively.

The generation terms ($R_{gen,i}$) that appear in the mass balance equations for every chemical species are calculated from Equations (1)–(11) by molar balances [4,19]. The equations to calculate all generation terms ($R_{gen,i}$) are given in the Appendix. All information related to the reaction scheme appears in the Appendix. Table A1 includes all chemical compounds. The values of all kinetic parameters used in this work are listed in Table A2.

2.3. Reactive Mass Transfer

The two-film model is used to account for gas-liquid reactive mass transfer. This model assumes the presence of two stagnant thin layers on both sides of the gas-liquid interphase. Mass transfer occurs by molecular diffusion through the two thin layers [27]. Two mass transfer coefficients, one in each thin layer (k_g and k_l), are defined by the model. The presence of a chemical reaction increases mass transport, which is calculated by using an enhancement factor (E) [28].

The ionic species always remain in liquid phase, while the gaseous and volatile chemical compounds move between both phases. Gas-phase only mass transfer resistance is considered for water while liquid only mass transfer resistance applies to the other gas species. However, both resistances must be considered for CO_2 . In our model, we consider this situation by using a global mass transfer coefficient given by,

$$\frac{1}{K_{CO_2}^l} = \frac{1}{E k_{CO_2}^l} + \frac{H^{cc}}{k_{CO_2}^g}. \quad (12)$$

Here, $K_{CO_2}^l$ is the overall mass transfer coefficient based upon liquid phase concentrations, $k_{CO_2}^l$ is the liquid phase mass transfer coefficient, $k_{CO_2}^g$ is the gas phase mass transfer coefficient, $H^{cc} = C_i^l/C_i^g$, is the concentration based Henry's constant, C_i^l and C_i^g , are the liquid and gas phase i -species concentrations, respectively, and E is the enhancement factor. The enhancement number is a function of the dimensionless Hatta (Ha) number, which is a ratio of the component mass transfer with and without chemical reaction. When $Ha > 2$, the enhancement factor E is equal to the Ha number [28] so, the CO_2 molar flow term ($N_{CO_2,diff}$) is calculated by [4,29,30]:

$$N_{CO_2,diff} = -k_{CO_2}^l E a_w H^{cc} C_{CO_2}^g. \quad (13)$$

Here, a_w is the gas-liquid interphase area per unit volume.

2.4. Slurry Bubble Column Model

2.4.1. Mass Balances

A mass balance for the i -component in the liquid-phase of the slurry bubble column shown in Figure 1 is given by [4,19,30],

$$\frac{\partial C_i^l}{\partial t} = D_1 \frac{\partial^2 C_i^l}{\partial z^2} + u_l \frac{\partial C_i^l}{\partial z} - N_{i,diff} - k_{s,i} a_s (C_i^l - C_i^s) + R_{gen,i}^l. \quad (14)$$

Here, u_l is the liquid phase superficial velocity, D_1 is the liquid phase dispersion coefficient, C_i^s is the volumetric concentration of the i -component on the liquid-solid interface, a_s is the solid-phase holdup, and $k_{s,i}$ is the liquid to solid phase mass transfer coefficient for the i -component. Replacing Equation (14), the interfacial liquid-gas mass transfer ($N_{i,diff}$) using Equation (25) in reference [19] leads to,

$$\frac{\partial C_i^l}{\partial t} = D_1 \frac{\partial^2 C_i^l}{\partial z^2} + u_l \frac{\partial C_i^l}{\partial z} + k_{l,i} a_w (C_i^{l,*} - C_i^l) - k_{s,i} a_s (C_i^l - C_i^s) + R_{gen,i}^l. \quad (15)$$

Here, $k_{l,i}$ is the i -component gas-liquid mass transfer coefficient, $C_i^{l,*}$ is the equilibrium gas-liquid interface concentration of the i -component, and C_i^l is the i -component liquid phase concentration.

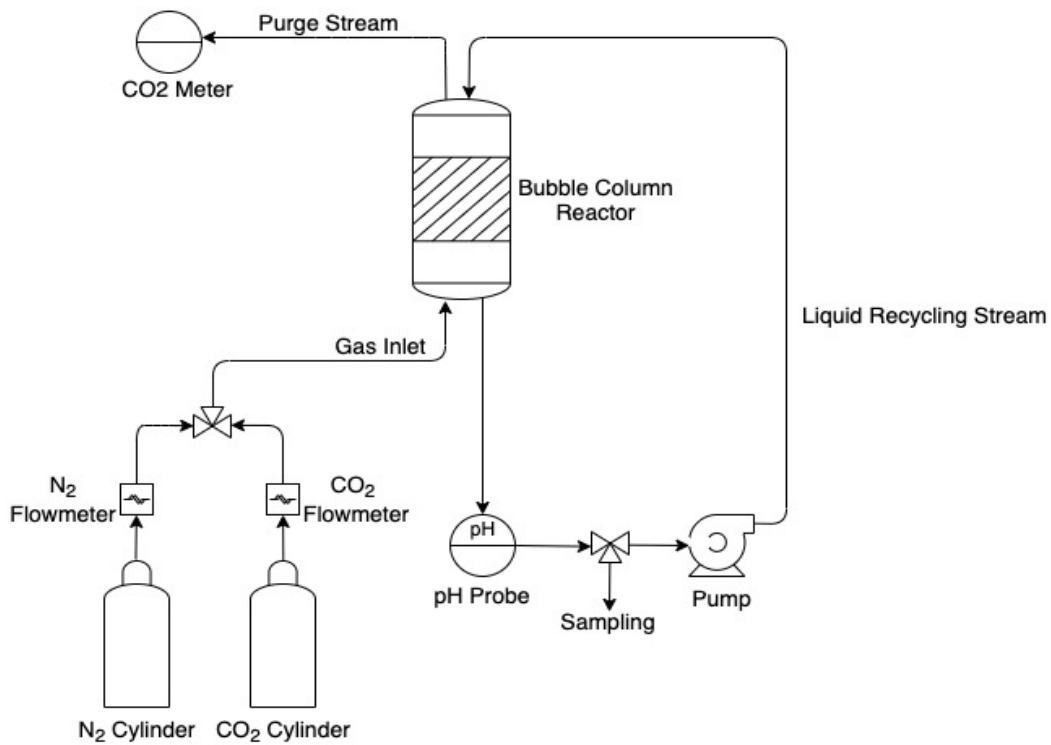


Figure 1. Experimental setup used for CO₂ absorption experiments.

At steady state, a mass balance for the *i*-component in the liquid-solid interface is given by,

$$k_{s,i} a_s (C_i^l - C_i^s) - a_s R_{gen,i}^s = 0. \quad (16)$$

Here, $R_{gen,i}^s$ is the production of the *i*-component by reaction at the liquid-solid interface. These generation terms affect only the chemical species that participate in the precipitation reaction, Equations (8) and (9). Introducing Equation (16) into (15) leads to,

$$\frac{\partial C_i^l}{\partial t} = \left\{ D_l \frac{\partial^2 C_i^l}{\partial z^2} + u_l \frac{\partial C_i^l}{\partial z} \right\} + k_{l,i} E a_w (C_i^{l,*} - C_i^l) - a_s R_{gen,i}^s + R_{gen,i}. \quad (17)$$

In the gas phase a mass balance for species-*i* leads to

$$\frac{\partial C_i^g}{\partial t} = D_g \frac{\partial^2 C_i^g}{\partial z^2} - u_g \frac{\partial C_i^g}{\partial z} + N_{i,diff}^l. \quad (18)$$

Here D_g is the gas phase dispersion coefficient. Replacing $N_{i,diff}^l$ in Equation (18) using [19] leads to,

$$\frac{\partial C_i^g}{\partial t} = D_g \frac{\partial^2 C_i^g}{\partial z^2} - u_g \frac{\partial C_i^g}{\partial z} - k_l a_w (C_i^{l,*} - C_i^l). \quad (19)$$

2.4.2. Parameter Estimation

The implementation of the slurry bubble column model requires the evaluation of several parameters including the overall gas hold-up ε_g , overall solid hold-up ε_s , the volumetric mass transfer coefficient $k_1 a_w$, the liquid side mass transfer coefficient k_l , the volumetric interfacial area a_w , the gas and liquid dispersion coefficients D_g and D_l , the bubble size d_{bs} , the bubble distribution throughout the column, and the solid GBIG distribution throughout the column. The model parameters required for simulation of the slurry bubble column were calculated using literature information [31–34]. Our slurry bubble column operates in the homogeneous regime characterized by small bubbles with

diameters between 1 and 7 mm and narrow bubble size distribution [34]. We also assumed homogeneous concentration of solid particles throughout the column. In some cases where literature data were not available, we used experimentally measured values of these parameters [22].

The average gas hold-up (ε_g) is calculated using [33],

$$\varepsilon_g = 0.00494 \frac{\rho_L^{0.42} \rho_G^{0.18}}{\mu_L^{0.17} \sigma_L^{0.27}} u_g^{0.55} \left(\frac{P_T}{P_T - P_S} \right)^{0.20} \left(\frac{D_C}{D_C + 1} \right)^{-0.12} \Gamma^{0.05} \exp(-2.23 C_v - 0.16 \rho_p d_p - 0.24 X_w). \quad (20)$$

Here, D_C is the column diameter, P_T is the total pressure, P_S is the saturation vapor pressure, u_G is the superficial gas velocity, ρ_G is the gas density, ρ_L is the liquid phase density, μ_L is the liquid phase viscosity, σ_L is the liquid phase surface tension, ρ_p is the solid particles density, d_p is the solid particles diameter, ρ_p is the solid particles density, C_v is the volumetric solid concentration, X_w is the mass percentage of the solvent in a liquid mixture, and Γ is the sparger coefficient calculated using,

$$\Gamma = K_d N_O d_O^\alpha. \quad (21)$$

Here, K_d is a sparger constant, N_O is the number of distributor orifices, d_O is the diameter of the distributor orifices, and the exponent α is constant calculated from Equation (26) in ref. [33].

The specific gas-liquid interphase area (a_w) is calculated using [32]:

$$a_w = \frac{6 \varepsilon_g}{(1 - \varepsilon_g) d_{bs}}. \quad (22)$$

The Sauter mean diameter of the bubbles (d_{bs}) is given by [32],

$$d_{bs} = 37.19 \frac{\mu_L^{0.08} \sigma_L^{0.22} \rho_G^{0.02}}{\rho_L^{1.52} M_{w-gas}^{0.12}} u_g^{0.14} \left(\frac{D_C}{D_C + 1} \right)^{0.30} (1 - \varepsilon_g)^{1.56} \Gamma^{-0.02} \exp(2.81 C_v + 2.77 \rho_p d_p - 2.29 X_w). \quad (23)$$

The liquid-layer mass transfer coefficient ($k_l a_w$) is calculated from [34]:

$$\frac{k_l a_w}{(1 - \varepsilon_g)} = 6.14 \times 10^4 \frac{\mu_L^{0.12} \rho_L^{0.26} \varepsilon_G^{1.21} D_{AB}^{0.50}}{\sigma_L^{0.52} \rho_G^{0.06} u_G^{0.12} d_{bs}^{0.05} T^{0.68}} \left(\frac{D_C}{D_C + 1} \right)^{0.40} \Gamma^{-0.11}. \quad (24)$$

Here, D_{AB} is the diffusivity of A-species into the liquid phase.

The liquid axial dispersion coefficient (D_L) is given by [33]:

$$D_L = 0.35 D_c^{4/3} (g u_g)^{1/3}. \quad (25)$$

Since the gas bubbles in the homogeneous regime are relatively small, we assumed that the gas bubbles dispersion coefficient is equal to the liquid dispersion coefficient [35], ($D_G \cong D_L$).

2.5. Experimental Part

Experimental data were measured using the experimental set-up reported by Kasturi et al. [17] as shown in Figure 1. In our experiments we prepared 3 L of 1 M potassium hydroxide purchased from Fisher Chemicals (Fair Lawn, NJ, USA) by dilution of a 45 weight% potassium hydroxide solution. We promoted diluted potassium hydroxide solutions by mixing 1 M equivalent of sarcosine. We purchased sarcosine (>99% purity) from Sigma Aldrich (Milwaukee, WI, USA). We prepared a simulated flue gas stream by combining individual gaseous streams of CO_2 and N_2 obtained from their respective gas cylinders purchased from Airgas (Atlanta, GA, USA). The input 14% (v/v) CO_2 stream was prepared by adjusting the flow rates of CO_2 and N_2 until the desired values were obtained.

The total gas flowrate was 5 Lmin^{-1} . Liquid samples were taken at the bottom of the bubble column reactor and then analyzed for total carbonate concentration using a Dionex ICS-5000+ ion chromatography and for pH using an Acumet 50 pH-meter. The output CO_2 gaseous concentration at the top of the column was measured using a CM-0003 CO_2 m from CO2Meter (Ormond Beach, FL, USA). Experimental data were used to support and validate process simulations. We measured gas and solid hold-up values (e_g and e_s) by taking pictures of the column sections at different times.

3. Results and Discussion

The model presented in the theoretical section was implemented by modifying the custom-made FORTRAN computer code developed by Gabitto et al. [19,22]. More details can be found in the references. The experimental data from Kasturi et al. [17] showed that the bubble diameter changes with position and time in a very complex way. The presence of the solid phase introduces further changes in gas bubble size and distribution. A simulation model considering the formation and coalescence of bubbles is needed for accurate simulation of this behavior. Such a model, however, is beyond the scope of this work. Therefore, it was decided to fit the experimental data using a constant bubble diameter for the whole experiment instead of trying complex functions of bubble size with axial position and time. Typical results are plotted in Figures 2–5. The operating values used in the simulations are shown in Table A3 in the Appendix.

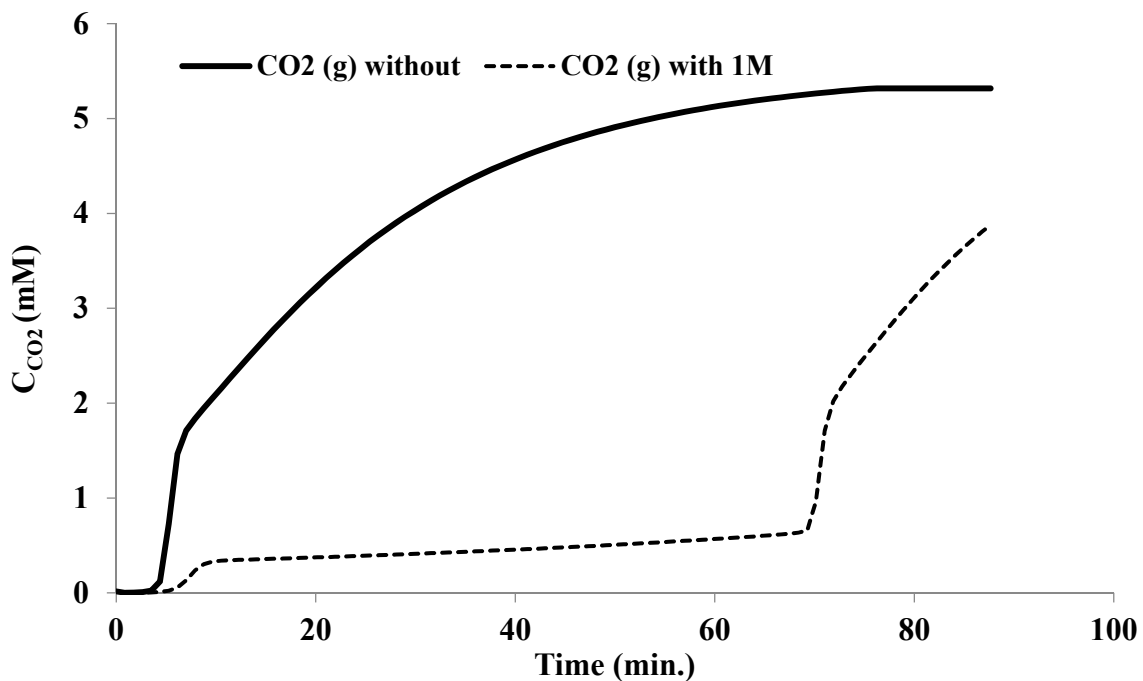


Figure 2. Time variation of CO_2 concentration in gas phase measured at exit stream with and without GBIG.

Figure 2 shows typical values of exit CO_2 concentration in gas phase vs. time with and without GBIG. The designation “without” means no GBIG is present in the system; therefore, no $\text{GBIGH}_2^+ (\text{HCO}_3^-)_2 (\text{H}_2\text{O})_2$ solid precipitates. The simulation results show that the presence of the guanidine compound significantly delays breakthrough behavior compared with the case without the guanidine compound. The area above both curves is proportional to the amount of CO_2 absorbed in liquid-phase; therefore, there is significantly more CO_2 absorbed when the guanidine compound is present. Several authors found that the CO_2 concentration in the gas phase decreases as the amino acid salt concentration increases due to the counterflow operation of the column [17,19]. However, caution needs to be exerted as in this work the experiments were run by continuously recycling the slurry phase. Therefore, as time increases, the input concentration of the amino acid salt at the

top of the column decreases while the gas phase input concentration at the bottom remains constant.

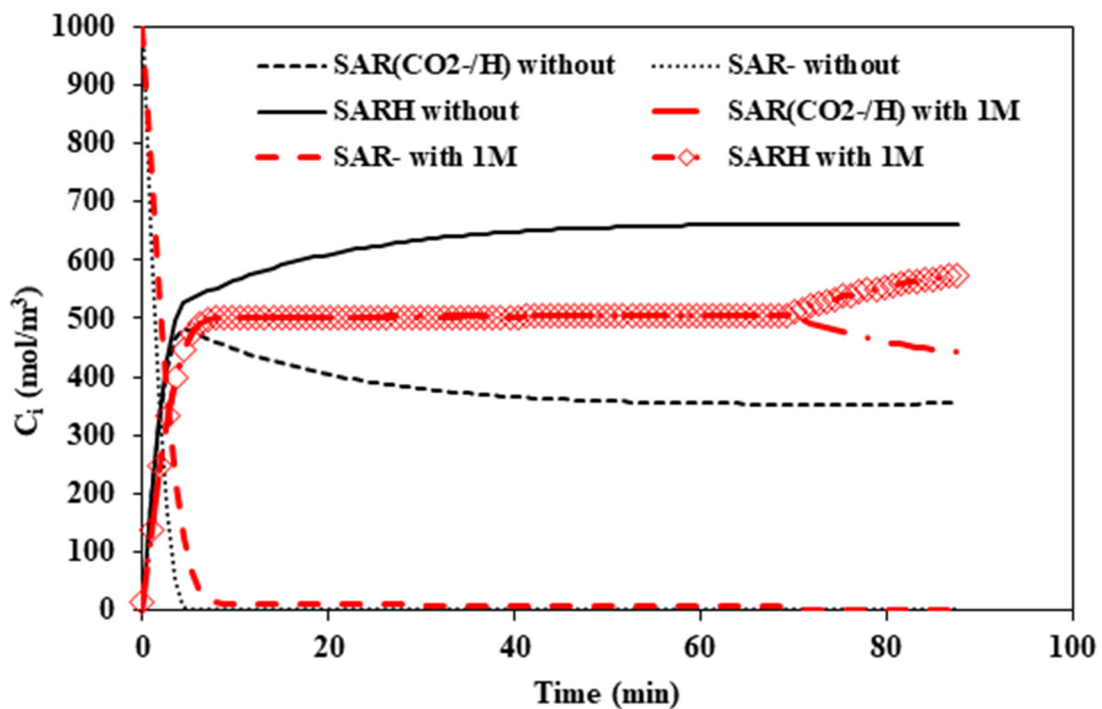


Figure 3. Time evolution of amino acid compounds in liquid phase, red with GBIG present, black without GBIG present.

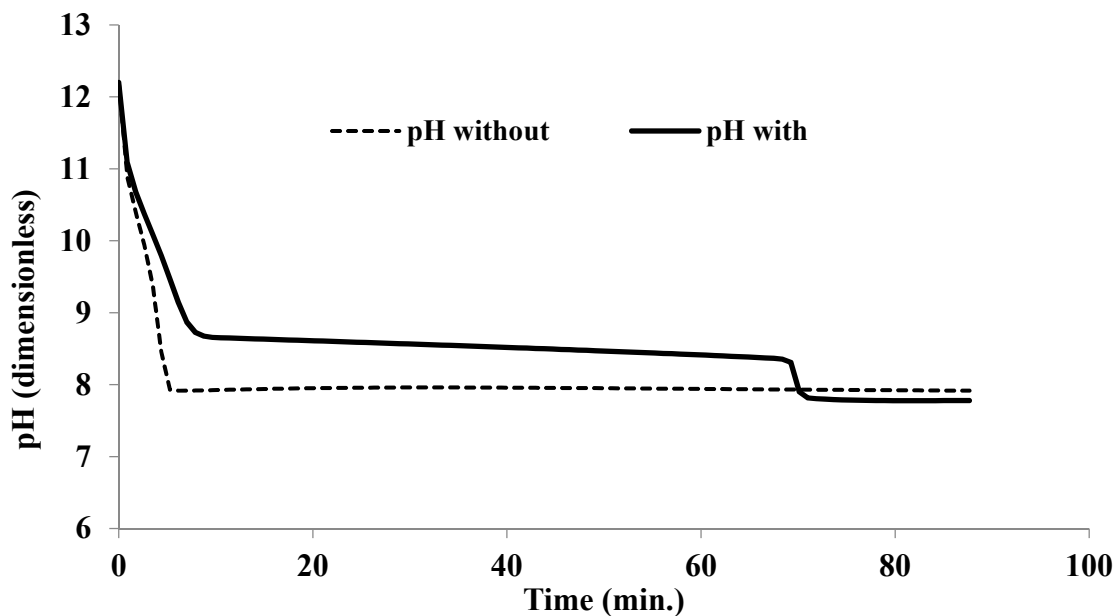


Figure 4. pH variation with time with and without GBIG present.

Kasturi et al. [17,22] reported that the values of the concentration of the different amino acid forms, the concentration of the products of the different reactions with CO_2 , and the pH are strongly related. The simulation results are shown in Figures 3–5.

Figure 3 shows the time variation of the concentration of the different amino acid compounds at the bottom of the column. The predominant form of the amino acid at high pH is the alkaline salt (SAR^-). This compound is consumed throughout the column by reaction with CO_2 to produce the carbamate form, $\text{SAR}^-(\text{CO}_2^-)$. The amino acid

concentration (SAR^-) is higher with GBIG present than without. It is shown in Figure 3 that the total carbamate ($\text{SAR}^- \text{CO}_2^- / \text{SAR}^- \text{CO}_2\text{H}$) concentration is significantly higher with than without GBIG present. This ratio is equal to the stoichiometric ratio, Equation (1), with GBIG present while it is smaller without. After consumption of GBIG the system reverts to the behavior without GBIG.

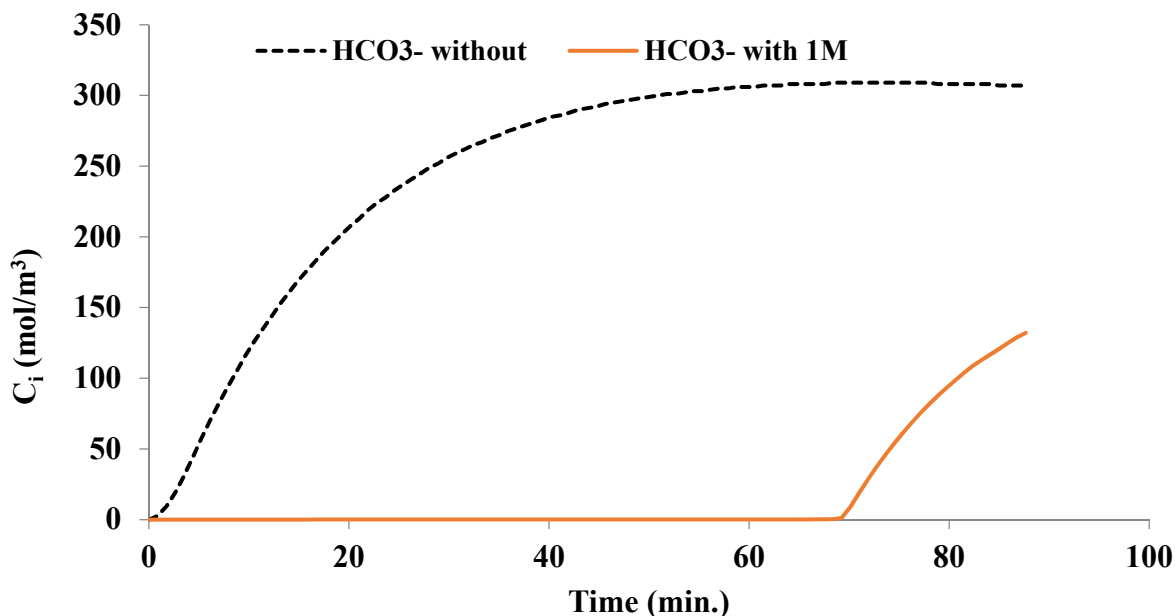


Figure 5. HCO_3^- concentration as a function of time with and without GBIG.

The simulation results depicted in Figure 4 show that the pH value at the column bottom drops fast with time as the amino acid salt is consumed. After a high decrease in the amino acid concentration the pH remains relatively constant. When GBIG is consumed the pH decreases up to similar values than without GBIG present. We can also see that the pH is higher with GBIG present than without.

Figure 5 shows the variation of the concentration of HCO_3^- with time. The presence of GBIG significantly delays bicarbonate increase in liquid phase. When GBIG is present HCO_3^- is consumed to form the carbonated GBIG precipitate. As the amount of GBIG is entirely consumed the system behaves similarly to the case without GBIG. Inspection of the results reported in Figure 4 shows that the pH decrease is caused by the bicarbonate ion concentration increase.

The simulation results shown in Figures 2–5 show that the decrease in CO_2 absorption with time is produced by the decrease in the concentration of the alkaline form of the amino acid. This decrease is produced by formation of a carbamate compound, and by the decrease in pH which favors the formation of the protonated form of the amino acid, as shown in Figure 3. The simulation results shown in Figures 2–5 lead us to propose the following description of the CO_2 absorption process. At short times, a big amount of CO_2 is absorbed by carbamate formation. This process is fast and in approximately 10 min most of the amino acid has been transformed into the carbamate form by the reaction given by Equation (1) or into the protonated form of the amino acid due to the decrease in pH. The protonated form of the amino acid does not actively participate in CO_2 absorption [26]. This step produces a significant decrease in the pH value. The results presented in Figure 2 show that after this period ends there is a sharp increase in CO_2 concentration without GBIG present while in the presence of GBIG the CO_2 concentration remains relatively constant. CO_2 is still absorbed by the alkaline aqueous solution, Equation (6); however, this step is relatively slow and produces only a slight decrease in pH, but neither the concentration of bicarbonate increases, nor the pH decreases further because the guanidine compound reacts with HCO_3^- to produce the carbonated precipitate and regenerates some amino acid

salt. This step produces the slight increase in the exit gaseous CO_2 concentration shown in Figure 2 from time = 10 to 70 min in the presence of GBIG. After 70 min, the amount of the guanidine compound has been significantly reduced and the system behaves as the system without guanidine. Changes in bubble size and bubble size distribution can also affect the behavior observed in these simulation results.

The presented simulation results established qualitative trends for the variation of the main chemical compounds participating in the complex reactions associated with the CO_2 absorption by amino acid salts. Quantitative agreement between simulation results and experimental data can only be achieved by using the bubble size as an adjustable parameter because the model presented in this work lacks a subroutine to calculate bubble size and bubble size distributions. The comparison of our simulation results with Kasturi et al. [22] is shown in Figures 6 and 7.

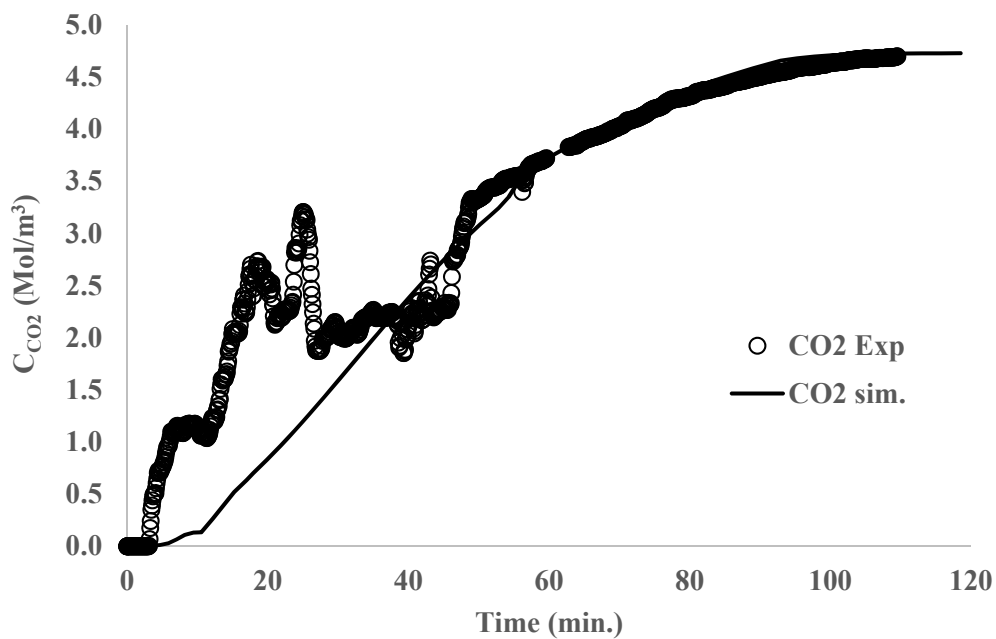


Figure 6. Comparison between experimental data and simulation results.

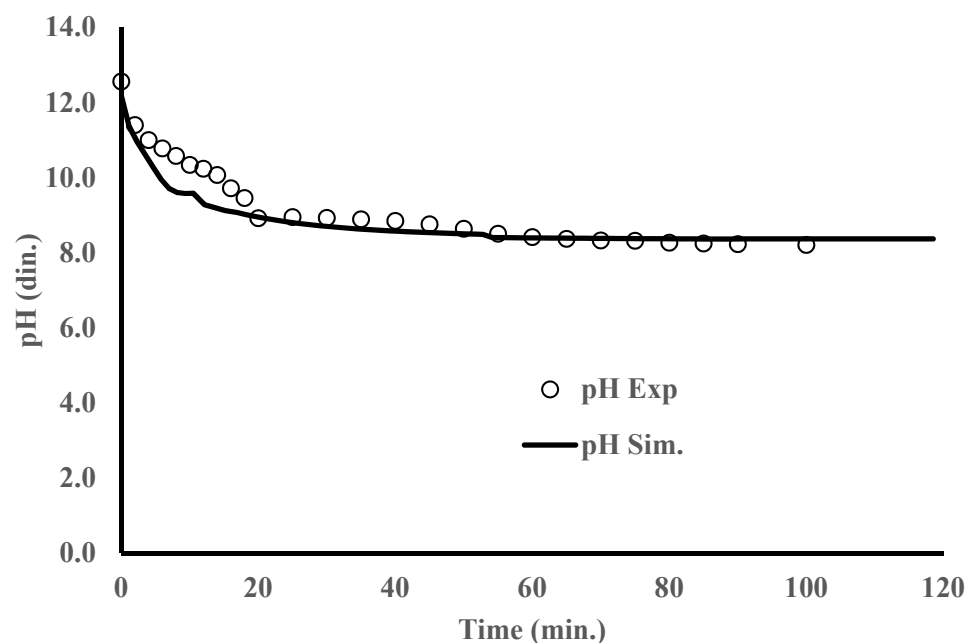


Figure 7. Comparison of the time variation of pH for experimental data and simulation results.

Figure 6 shows good agreement between experimental data and simulation results for very short and long times. At intermediate times, from 4 to 40 min, the agreement is not as good. The variation in bubble size distribution with time and position was considered the reason behind the difference in experimental and simulation results at intermediate time scales. Kasturi et al. [22] reported similar results for experiments without the presence of the guanidine compound.

A comparison with experimental results for pH is shown in Figure 7. The simulation results depicted in the Figure show that there is very good agreement for very short and long times. However, once again there is only fair agreement for intermediate times, from 4 to 20 min. A theoretical model that calculates bubble sizes and distributions is needed to improve the predictions.

4. Conclusions

A simulation model for CO₂ capture in a slurry bubble column combining an absorption step and a regeneration step has been developed. The model has been implemented by writing a custom-made computer code. The interactions among amino acid forms, pH, and different carbonated products have been studied. Breakthrough behavior for output carbon dioxide concentration in gas phase has been observed. The breakthrough behavior is produced by significant amino acid consumption and pH decrease at very short times. Simulation results and experimental data agree well for very short and long periods of time. The agreement is only fair at intermediate times. The lack of a theoretical model that represents the bubble size changes with time and position is considered the reason for the discrepancy at intermediate times. Comparison between simulation results and experimental data with and without the guanidine compound (GBIG) shows that the presence of the guanidine compound significantly increases the amount of CO₂ captured and the pH. The increase in pH and the precipitation of the extra amount of bicarbonate ion formed by alkaline absorption are considered the main reasons for the improved operation.

In conclusion, the results presented in this work show that it is possible to implement a combined CO₂ sequestration and amino acid regeneration process with improved efficiency compared to a process without simultaneous regeneration. It should also be emphasized that, although the model and experiments were performed using a bubble column, the same conclusions are applicable for other types of absorbers, such as packed columns, which are designed to operate with lower pressure drop.

Author Contributions: A.K. participated in investigation and visualization; J.F.G. participated in methodology, software, validation, and writing—original draft; R.C. participated in conceptualization, funding acquisition, and writing—review and editing; and C.T. participated in conceptualization, funding acquisition, project supervision, and writing—review and editing. All authors have read and agreed to the published version of the manuscript.

Funding: This research was supported by the U.S. Department of Energy, Office of Technology Transitions, through a Technology Commercialization Fund supported by the Office of Fossil Energy and Carbon Management. Partial support (Jorge Gabitto) by a RISE Grant from the office of the Vice-President of Research at PVAMU is kindly acknowledged. This study was conducted at Prairie View A&M University and the Oak Ridge National Laboratory (ORNL). ORNL is managed by UT-Battelle, LLC under Contract No. DE-AC05-00OR22725 with the U.S. Department of Energy.

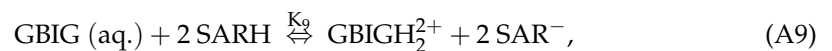
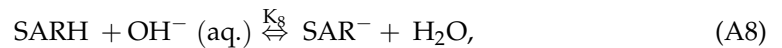
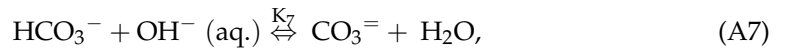
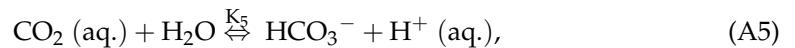
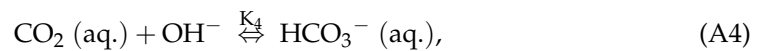
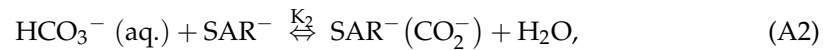
Data Availability Statement: See notice below concerning the policies from the USA government related to data generate in US agencies.

Conflicts of Interest: The authors declare no conflict of interest. This manuscript has been authored by UT-Battelle, LLC under Contract No. DE-AC05-00OR22725 with the U.S. Department of Energy. The United States Government retains and the publisher, by accepting the article for publication, acknowledges that the United States Government retains a non-exclusive, paid-up, irrevocable, world-wide license to publish or reproduce the published form of this manuscript, or allow others to do so, for United States Government purposes. The Department of Energy will provide public

access to these results of federally sponsored research in accordance with the DOE Public Access Plan. (<http://energy.gov/downloads/doe-public-access-plan>).

Appendix

Reactions



Generation Terms

Assuming the pseudo-steady state for every chemical species, we can calculate the generation terms that appear in the chemical species mass balances. To simplify the calculations, we determined an overall rate per reaction according to,

$$R_{ai} = r_{if} - r_{ir}. \quad (\text{A11})$$

Every generation term (R_{geni}) is calculated by a molar balance using:

$$R_{gen1} = -R_{a1} - 2 R_{a2} + R_{a8} + 2 R_{a9} (\text{SAR}^-), \quad (\text{A12})$$

$$R_{gen2} = R_{a1} + R_{a2} - R_{a3} (\text{SAR}^-(\text{CO}_2^-)), \quad (\text{A13})$$

$$R_{gen3} = R_{a3} \text{SAR}^-(\text{CO}_2\text{H}), \quad (\text{A14})$$

$$R_{gen4} = -R_{a1} - R_{a4} - R_{a5} \text{CO}_2 (\text{aq.}), \quad (\text{A15})$$

$$R_{gen5} = 0 \text{H}_2\text{O}, \quad (\text{A16})$$

$$R_{gen6} = -R_{a2} - R_{a7} - 2 R_{a10} + R_{a4} + R_{a5} (\text{HCO}_3^-), \quad (\text{A17})$$

$$R_{gen7} = R_{a6} - R_{a4} - R_{a7} - R_{a8} (\text{OH}^-), \quad (\text{A18})$$

$$R_{gen8} = -R_{a3} + R_{a5} + R_{a6} (\text{H}^+), \quad (\text{A19})$$

$$R_{gen9} = R_{a7} (\text{CO}_3^{2-}), \quad (\text{A20})$$

$$R_{gen10} = R_{a1} - R_{a8} (\text{SARH}), \quad (\text{A21})$$

$$R_{gen11} = R_{a9} - R_{a10} (\text{GBIGH}_2^{2+}), \quad (\text{A22})$$

$$R_{gen12} = R_{a10} \left((\text{GBIGH}_2^{2+}) (\text{HCO}_3^-)_2 (\text{H}_2\text{O})_2 \right). \quad (\text{A23})$$

Table A1 lists all the chemical compounds participating in reactions (A1) to (A10).

Table A1. List of compounds participating in the reaction scheme.

Compound N°	Gas	Liquid
1	N ₂ (g)	SAR ⁻
2	O ₂ (g)	SAR ⁻ (CO ₂ ⁻)
3	CO ₂ (g)	SAR ⁻ (CO ₂ H)
4	H ₂ O (g)	CO ₂ (aq.)
5	-	H ₂ O
6	-	HCO ₃ ⁻
7	-	OH ⁻
8	-	H ⁺
9	-	CO ₃ ²⁻
10	-	SARH (aq.)
11	-	GBIGH ₂ ²⁺ (aq.)
12	-	GBIGH ₂ (HCO ₃) ₂ (H ₂ O) ₂

Kinetic Data

Table A2 summarizes all the kinetic parameters for the rate equations used in the model. The first number in the first column is the equation number used in the Appendix. The second number refers to the original equation number used in the article. (-) means that the equation has not been listed in the article, but it has been included in the model for completeness.

Table A2. Kinetic information used in solving the proposed reaction model.

Eqn. No/Reaction	Forward Rate (k _f)	Equilibrium Constant	Reverse Rate (k _r)
A1 (1 + 2)	$k_{1f} = 9.5 \times 10^{11} \text{ (mM}^{-1}\text{s}^{-1}) \times \exp(-7348/T_1)$	$K_1 = 11.78 \times \exp(721.7/T_1) \times 10^{(909.1/T_1)}$	$k_{1r} = k_{1f}/K_1$
A2 (4)	$k_{2f} = 3.59 \times 10^5 \text{ (mM}^{-1}\text{s}^{-1}) \times \exp(-7400/T_1)$	$K_2 = k_{2f}/k_{2r}$	$k_{2r} = 4931.6 \text{ (mM}^{-1}\text{s}^{-1}) \times \exp(-8004/T_1) \text{ (s}^{-1})$
A3 (5)	$k_{3f} = 4.52 \times 10^7 \text{ (mM}^{-1}\text{s}^{-1}) \times 10^{(-909.1/T_1)}$	$K_3 = 4.52E10 \text{ (M}^{-1}) \times 10^{(-909.1/T_1)} \text{ (mM}^{-1})$	$k_{3r} = (k_{3f})/K_3$
A4 (6)	$k_{4f} = 1.88 \times 10^{12} \times \exp[-7698./T_1] \text{ (mM}^{-1}\text{s}^{-1})$	$K_4 = k_{4f}/k_{4r}$	$k_{4r} = 2.491 \times 10^{16} \times \exp[-1.367E4/T_1] \text{ (s}^{-1})$
A5 (7)	$k_{5f} = 4.32 \times 10^{-7} \text{ (s}^{-1})$	$K_5 = 10^{(3404.7/T_1)} + 0.032786 \times T_1 + 14.8435 \text{ (mM)}$	$K_{5r} = (k_{5f})/K_6$
A6 (-)	$k_{6f} = 3.6 \times 10^{-10} \text{ (s}^{-1}\text{ mM)}$	$K_6 = 1.58 \times 10^{-3} \text{ (mM}^2) \times \exp(-6832/T_1)$	$k_{6r} = (k_{6f})/K_6$
A7 (-)	$k_{7f} = 0.1 \text{ (mM}^1\text{s}^{-1})$	$K_7 = 4.474 \times 10^{-3} \text{ (mM}^{-1}) \times \exp(5325./T)$	$k_{7r} = (k_{7f})/K_7$
A8 (-)	$k_{8f} = 0.1 \text{ (mM}^1\text{s}^{-1})$	$K_8 = 2.83 \times 10^{-5} \text{ (mM}^{-1}) \times \exp(6832./T)$	$k_{8r} = (k_{8f})/K_8$
A9 (8)	$k_{9f} = 2 \times 10^{-5} T_1 \text{ (mM}^{-2}\text{s}^{-1})$	$K_9 = 2.26 \times 10^{-5} \text{ (mM}^{-1})$	$k_{9r} = (k_{9f})/K_9$
A10 (9)	$k_{10f} = 8.95 \times 10^{-3} \text{ (mM}^1\text{s}^{-1})$	$K_{10} = 0.54 \text{ (mM}^{-3})$	$k_{10r} = (k_{10f})/K_{10}$

Simulation Parameters

Table A3 contains a list of the parameters and operating conditions used in our simulations.

Table A3. Values used in the simulations.

Notation	Parameter	Value/Range	Units
Q_g	Gas phase flow rate	1–5	L min ⁻¹
Q_l	Liquid phase flow rate	0.1–1	L min ⁻¹
L_c	Column height	0.9	m
D_C	Column diameter	0.08	m
d_{bs}	Gas bubble Sauter diameter	1×10^{-3} – 5×10^{-3}	m
V_S	Solid volume fraction	0.04–0.1	(-)
X_{g,CO_2}^0	Initial CO ₂ volume fraction in gas-phase	0.05–0.14	(-)
V_{Tank}	Liquid feed tank volume	0.5×10^{-3} – 4×10^{-3}	m ³
$C_{l,SAR}^0$	Initial amino acid concentration	0.1–1	M
$C_{l,GBIG}^0$	Initial GBIG concentration	0.1–1	M
P_T	Total pressure	1.1×10^{-5}	Pa
T	Temperature	293	K
pH	Potential of hydrogen	10.2–12.5	(-)

References

1. Masson-Delmotte, V.; Zhai, P.; Pörtner, H.O.; Roberts, D.; Skea, J.; Shukla, P.R.; Pirani, A.; Moufouma-Okia, W.; Péan, C.; Pidcock, R.; et al. *Global Warming of 1.5 °C*; An IPCC Special Report on the Impacts of Global Warming of 1.5 °C above Pre-Industrial Levels and Related Global Greenhouse Gas Emission Pathways, in the Context of Strengthening the Global Response to the Threat of Climate Change, Sustainable Development, and Efforts to Eradicate Poverty; IPCC: Geneva, Switzerland, 2018.
2. Blunden, J.; Arndt, D.S. State of the climate in 2018. *Bull. Am. Meteorol. Soc.* **2019**, *100*, Si–S306. [[CrossRef](#)]
3. Aaron, D.; Tsouris, C. Separation of CO₂ from Flue Gas: A Review. *Sep. Sci. Technol.* **2005**, *40*, 321–348. [[CrossRef](#)]
4. Greer, T. Modeling and Simulation of Post Combustion CO₂ Capturing. Master's Thesis, Telemark University College, Faculty of Technology, Porsgrunn, Norway, 2008.
5. Bosch, H.; Versteeg, G.F.; van Swaaij, W.P.M. Gas-Liquid Mass Transfer with Parallel Reversible Reactions-III. Absorption of CO₂ into Solutions of Blends of Amines. *Chem. Eng. Sci.* **1989**, *44*, 2745–2750. [[CrossRef](#)]
6. Hagewiesche, D.P.; Ashour, S.S.; Al-Ghawas, H.A.; Sandall, O.C. Absorption of Carbon Dioxide into Aqueous Blends of Monoethanolamine and Methyl-diethanolamine. *Chem. Eng. Sci.* **1995**, *50*, 1071–1079. [[CrossRef](#)]
7. Sakwattanapong, R.; Aroonwilas, A.; Veawab, A. Reaction Rate of CO₂ in Aqueous MEA-AMP Solution: Experiment and Modeling. *Energ. Procedia* **2009**, *1*, 217–224. [[CrossRef](#)]
8. Gabitto, J.; Tsouris, C. Carbon Dioxide Absorption Modeling for Off-Gas Treatment in the Nuclear Fuel Cycle. *Int. J. Chem. Eng.* **2018**, *2018*, 3158147. [[CrossRef](#)]
9. Versteeg, G.F.; Holst, J.V.; Politiek, P.P.; Niederer, J.P. CO₂ Capture from Flue Gas using Amino Acid Salt Solutions [Online], June 2006. Available online: <http://www.co2-cato.nl/doc.php?lid=317> (accessed on 4 September 2018).
10. van Holst, J.; Versteeg, G.F.; Brilman, D.W.F.; Hogendoorn, J.A. Kinetic Study of CO₂ with Various Amino Acid Salts in Aqueous Solution. *Chem. Eng. Sci.* **2009**, *64*, 59–68. [[CrossRef](#)]
11. Vaidya, P.D.; Konduru, P.; Vaidyanathan, M.; Kenig, E.Y. Kinetics of Carbon Dioxide Removal by Aqueous Alkaline Amino Acid salts. *Ind. Eng. Chem. Res.* **2010**, *49*, 11067–11072. [[CrossRef](#)]
12. Portugal, A.F.; Derks, P.W.J.; Versteeg, G.F.; Magalhães, F.D.; Mendes, A. Characterization of Potassium Glycinate for Carbon Dioxide Absorption Purposes. *Chem. Eng. Sci.* **2007**, *62*, 6534–6547. [[CrossRef](#)]
13. Shen, S.; Yang, Y.N.; Bian, Y.; Zhao, Y. Kinetics of CO₂ Absorption into Aqueous Basic Amino Acid Salt: Potassium Salt of Lysine Solution. *Environ. Sci. Technol.* **2016**, *50*, 2054–2063. [[CrossRef](#)] [[PubMed](#)]
14. Benamor, A.; Jaber Al-Marri, M.; Khraisheh, M.; Nasser, M.S.; Tontiwachwuthikul, P. Reaction Kinetics of Carbon Dioxide in Aqueous Blends of N-methyl-diethanolamine and Glycine using the Stopped Flow Technique. *J. Nat. Gas Sci. Eng.* **2016**, *33*, 186–195. [[CrossRef](#)]

15. Mahmud, N.; Benamor, A.; Nasser, M.S.; Al-Marri, M.J.; Qiblawey, H.; Tontiwachwuthikul, P. Reaction Kinetics of Carbon Dioxide with Aqueous Solutions of L-Arginine, Glycine & Sarcosine using the Stopped Flow Technique. *Int. J. Greenh. Gas Control* **2017**, *63*, 47–58.
16. Brethomé, F.M.; Williams, N.J.; Seipp, C.A.; Kidder, M.K.; Custelcean, R. Direct Air Capture of CO₂ via Aqueous-Phase Absorption and Crystalline-Phase Release using Concentrated Solar Power. *Nat. Energy* **2018**, *3*, 553–559. [[CrossRef](#)]
17. Kasturi, A.S.; Ladshaw, A.; Yiacoumi, S.; Gabitto, J.; Garrabrant, K.; Custelcean, R.; Tsouris, C. CO₂ Absorption from Simulated Flue Gas in a Bubble Column. *Sep. Sci. Technol.* **2019**, *54*, 2034–2046. [[CrossRef](#)]
18. Jockenhövel, T.; Schneider, R.; Rode, H. Development of an Economic Post-Combustion Carbon Capture Process. *Energy Procedia* **2009**, *1*, 1043–1050. [[CrossRef](#)]
19. Gabitto, J.; Custelcean, R.; Tsouris, C. Simulation of Carbon Dioxide Absorption by Amino Acids in Two-Phase Batch and Bubble Column Reactors. *Sep. Sci. Technol.* **2019**, *54*, 2013–2025. [[CrossRef](#)]
20. Seipp, C.A.; Williams, N.J.; Kidder, M.K.; Custelcean, R. CO₂ Capture from Ambient Air by Crystallization with a Guanidine Sorbent. *Angew. Chem. Int. Ed. Engl.* **2017**, *56*, 1042–1045. [[CrossRef](#)] [[PubMed](#)]
21. Williams, N.J.; Seipp, C.A.; Brethomé, F.M.; Ma, Y.-Z.; Ivanov, A.S.; Bryantsev, V.S.; Kidder, M.K.; Martin, H.J.; Holguin, E.; Garrabrant, K.A.; et al. CO₂ Capture via Crystalline Hydrogen-Bonded Bicarbonate Dimers. *Chem* **2019**, *5*, 719–730. [[CrossRef](#)]
22. Kasturi, A.; Gabitto, J.; Tsouris, C.; Custelcean, R. Carbon Dioxide Capture with Aqueous Amino Acids: Mechanistic Study of Amino Acid Regeneration by Guanidine Crystallization and Process Intensification. *Sep. Purif. Technol.* **2021**, *271*, 118839. [[CrossRef](#)]
23. Kim, Y.-H.; Park, L.K.; Yiacoumi, S.; Tsouris, C. Modular Chemical Process Intensification: A Review. *Annu. Rev. Chem. Biomol. Eng.* **2017**, *8*, 359–380. [[CrossRef](#)] [[PubMed](#)]
24. Simons, K.; Brilman, D.W.F.; Mengers, H.; Nijmeijer, K.; Wessling, M. Kinetics of CO₂ Absorption in Aqueous Sarcosine Salt Solutions: Influence of Concentration, Temperature, and CO₂ Loading. *Ind. Eng. Chem. Res.* **2010**, *49*, 9693–9702. [[CrossRef](#)]
25. Xiang, Q.; Fang, M.; Yu, H.; Maeder, M. Kinetics of the Reversible Reaction of CO₂ (aq) and HCO₃⁻ with Sarcosine Salt in Aqueous Solution. *J. Phys. Chem. A* **2012**, *116*, 10276–10284. [[CrossRef](#)] [[PubMed](#)]
26. Versteeg, G.F.; van Swaaij, W.P.M. On the Kinetics between CO₂ and Alkanolamines both in Aqueous and Non-Aqueous Solutions-I. Primary and Secondary Amines. *Chem. Eng. Sci.* **1988**, *43*, 573–585. [[CrossRef](#)]
27. Morsi, B.I.; Basha, O.M. Mass Transfer in Multiphase Systems. In *Mass Transfer-Advancement in Process Modelling*; Solecki, M., Ed.; IntechOpen: London, UK, 2017.
28. Perry, R.H.; Green, D.W. *Chemical Engineers Handbook*, 7th ed.; McGraw-Hill: New York, NY, USA, 1999.
29. Greer, T.; Bedelbayev, A.; Igreja, J.M.; Pereira Gomes, J.F.; Lie, B. A Dynamic Model for the De-Absorption of Carbon Dioxide from Monoethanolamine Solution. *Proc. SIMS* **2008**, *2008*, 7–8.
30. Tavlarides, L.L.; Lin, R.; Nan, Y.; Yiacoumi, S.; Tsouris, C.; Ladshaw, A.; Sharma, K.; Gabitto, J.; DePaoli, D. *Sorption Modeling and Verification for Off-Gas Treatment*; NEUP: Atlanta, GA, USA, 2015. Available online: <https://neup.inl.gov/> (accessed on 4 July 2021). [[CrossRef](#)]
31. Fukuma, M.; Muroyama, K.; Yasunishi, A. Properties of Bubble Swarms in a Slurry Bubble Column. *J. Chem. Eng. Jpn.* **1987**, *20*, 20–33. [[CrossRef](#)]
32. Lemoine, R.; Behkish, A.; Sehabiague, L.; Heintz, Y.; Oukaci, R.; Morsi, B.I. An Algorithm for Predicting the Hydrodynamic and Mass Transfer Parameters in Bubble Column and Slurry in Bubble Column Reactors. *Fuel Proc. Technol.* **2008**, *29*, 322–343. [[CrossRef](#)]
33. Sehabiague, L.; Lemoine, R.; Behkish, A.; Heintz, Y.; Sanoja, M.; Oukaci, R.; Morsi, B.I. Modeling and Optimization of a Large-Scale Bubble Column Reactor for Producing 10,000 bbl/day of Fischer-Tropsch Liquid Hydrocarbons. *J. Chin. Inst. Chem. Eng.* **2008**, *38*, 169–179. [[CrossRef](#)]
34. Götz, M.; Lefevre, J.; Mörs, F.; Ortloff, F.; Reimert, R.; Bajohr, S. Novel Gas Holdup Correlation for Slurry Bubble Column Reactors Operated in the Homogeneous Regime. *Chem. Eng. J.* **2017**, *308*, 1209–1224. [[CrossRef](#)]
35. de Swart, J.W.A.; an Vliet, R.E.; Krishna, R. Size, Structure and Dynamics of ‘Large’ Bubbles in a Two-Dimensional Slurry Bubble Column. *Chem. Eng. Sci.* **1996**, *51*, 4619. [[CrossRef](#)]